3D printed polyurethane honeycombs for repeated tailored energy absorption

Simon R. G. Bates[1], Ian R. Farrow[2], Richard S. Trask[3]

[1, 2] Advanced Composites Centre for Innovation and Science (ACCIS),
Department of Aerospace Engineering, University of Bristol, Queens Building,
University Walk, Bristol, BS8 1TR, UK.

[3] Department of Mechanical Engineering, University of Bath,
Claverton Down, Bath, BA2 7AY, UK.

[1] Simon.R.G.Bates@bristol.ac.uk

[2] Ian.Farrow@bristol.ac.uk

[3] R.S.Trask@bath.ac.uk

Abstract

Fused filament fabrication (FFF) 3D printing of thermoplastic polyurethanes (TPUs) offers a unique capability to manufacture tailorable, flexible cellular structures which can be designed and optimised for specific energy absorbing applications. This paper describes the first application of this methodology in the creation and experimental analysis of 3D printed cellular structures, which are capable of undergoing repeated compressions to densification without failure. A parametric study has been undertaken, capturing the energy absorbing capability of hexagonal arrays manufactured from two types of TPU, with relative densities 0.18-0.49. Arrays were subject to compressions at strain rates 0.03-0.3s^{-1} and were capable of absorbing energies over the range of 0.01-0.34J/cm^3, before recovering elastically. Critically, samples attained a maximum energy absorbing 'efficiency' of 0.36, which is comparable to that of traditional expanded closed cell polyurethane foams. The energy absorption behaviour of all structures was found to be dependent on strain rate and cell orientation with respect to the compression direction. This study shows the clear potential of FFF 3D printing for the creation of a new breed of cellular architectures, which are not constrained by existing manufacturing principles, offering the designer the capability to create resilient architectures specifically tailored to operational applications and environmental conditions.

Keywords: Cellular structures, thermoplastic polyurethane, 3D printing, energy absorption

Introduction:

Honeycomb structures have long been investigated for their use for energy absorption [1-4]. Traditional manufacturing methods, however, largely limit their complexity to regular repeating lattices, thus limiting the tailorability of their energy absorbing capabilities. 3D printing provides a geometric design freedom unrivalled by traditional manufacturing methods, coupled with the increased accessibility of this technology in recent years, this has allowed the creation of honeycombs with dual-material structures [5], structural hierarchy [6-8] and graded density [9]; these topological complexities all have the potential to enhance and tailor the energy absorbing capabilities of honeycombs. Much of the work in this field has focused on exploring the behaviour of rigid 3D printed honeycombs [6-9]; such structures subject to large compressive loads would fail by crushing and brittle fracture, preventing energy recovery or reuse. In order to utilise the advances in our understanding of honeycomb design in applications such as vibration isolation and personal protection equipment, it is necessary that the next generation of honeycomb structures be 3D printed from highly elastic, hard wearing materials.

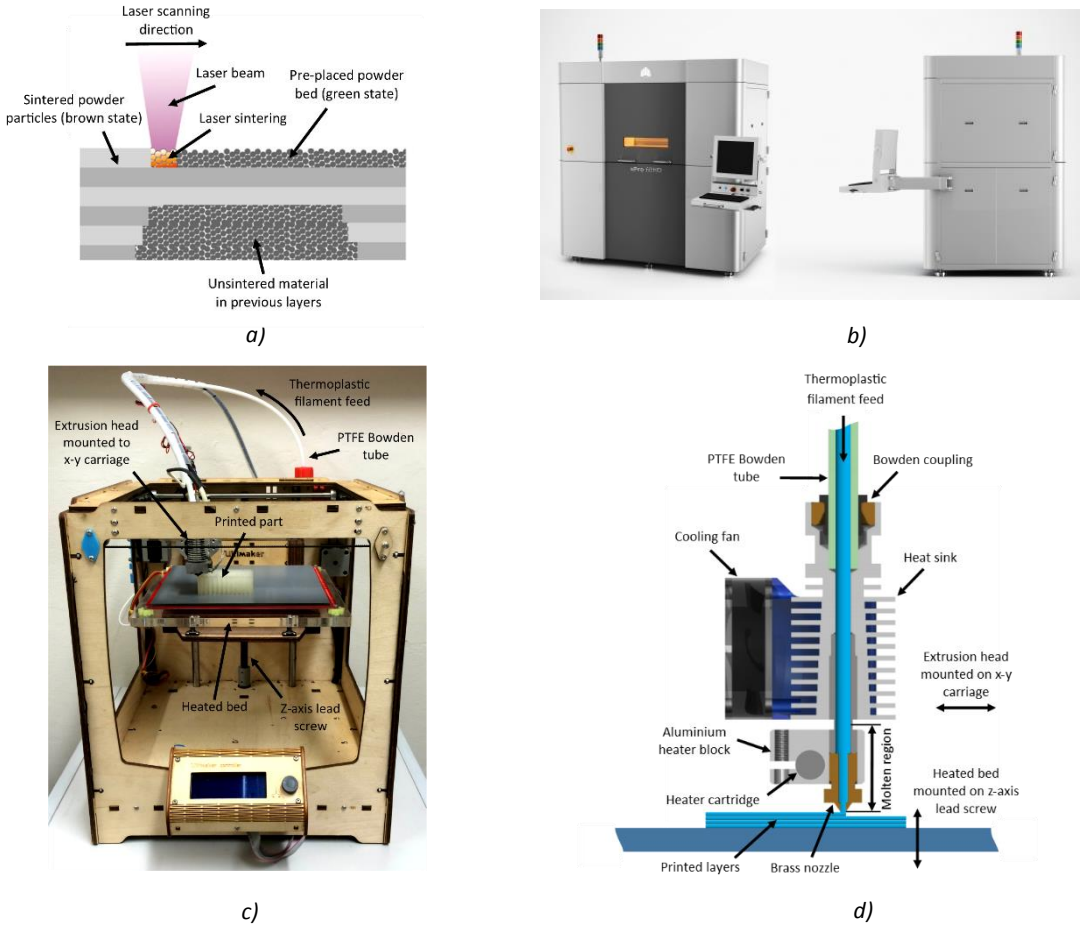

Figure 1: a) schematic detailing the laser sintering process, adapted from [11]; b) 3D systems sPro™60 HD SLS 3D printer [12]; c) Ultimaker Original 3D printer; d) a cut away schematic detailing the FFF print process, adapted from [13]

Materials which fit the criteria of flexibility have been developed and adapted for use in most 3D printing processes including fused filament fabrication (FFF), selective laser sintering (SLS), PolyJet and a number of other UV curing based techniques. Producing flexible parts via PolyJet 3D printing technology is attractive as the UV curing resins may be printed to a high resolution and dissolvable support material allows the manufacture of complex geometries. Despite these merits, the material

which forms the basis of the PolyJet flexible material range has a Young's modulus of less than 1Mpa [10] and tensile strength of 1.2Mpa [5] and therefore is extremely limited in its usefulness in energy absorbing applications; in work by Shen *et al* [10], auxetic lattices were created which failed during the extraction of the part from the surrounding support structure.

Thermoplastic polyurethanes (TPUs), however, are known to have excellent impact properties and abrasion resistance [14] and therefore are excellent candidates for parent materials in energy absorbing structures. TPUs can be processed in the same manner as traditional thermoplastics [14] and therefore may be printed by SLS or FFF 3D printing. The process of SLS 3D printing, as depicted in Figure 1a, involves sintering thin layers of powdered material with a laser beam. During this process, the selective scanning and discrete bonding of individual particles or clusters of particles imparts porosity [15]; this porosity is undesirable in most cases as it will degrade the properties of the structure and the exact porosity of the final part is hard to predict. Due to the requirement of high precision and use of high powered lasers, SLS 3D printers are generally large, industrial machines such as the sPro^{TM} 60 HD produced by 3D Systems, shown in Figure 1b.

FFF 3D printers on the other hand do not require the same power or high precision processes to produce 3D printed components and therefore can be built for a considerably lower cost and are much more easily modified; Figure 1c shows the Ultimaker Original FFF 3D printer used in this work, which is one such printer. The FFF print process which is detailed in Figure 1d involves the deposition of molten layers of thermoplastic in a predetermined manner to construct objects. Although the surface finish of parts produced by FFF have been shown to be inferior to that of those produced by other 3D printing methods [16], a lower porosity may be achieved when compared to the SLS process, making it a more attractive process for producing structural parts. It must also be noted that the surface finish and dimensional tolerance of FFF 3D printed parts may be vastly improved via the manipulation of printer variables such as layer height and nozzle diameter. In work by Kim and Oh [16] it was shown that FFF 3D printing using a layer thickness of 0.254mm produced the roughest surface finish when compared to other 3D printing techniques however, for example, the Ultimaker Original 3D printer is capable of printing with a layer thickness of just 20 microns [17]; using this layer height would increase print time but greatly reduce surface roughness and improve design tolerance.

As well as the surface finish and tolerance achievable, when selecting an appropriate 3D printing process for a component, the complexity and use of the final 3D printed part must also be considered. For the production of practical cellular structures, SLS 3D printing limits structures to an open cell form as the base material would become trapped within any closed cells and could not be removed in post-processing. Further, unlike SLS 3D printing, FFF also allows the printing of multiple materials in a single part by using multiple feedstock materials. This capability is of importance as the targeted placement of materials with varying stiffness within a cellular structure provides a useful method for structural tailoring; in work by Wang *et al.* [5], favourable deformations of auxetic lattices were achieved in this way using multi-material PolyJet 3D printing.

In this work, we investigate the potential of FFF 3D printing of TPU for the manufacture of recoverable energy absorbing structures with tailorable properties. In this instance, the structures will take the form of single density hexagonal arrays, allowing their potential to be assessed before topological complexity allowed by the 3D printing process is included in future work. The effect of manipulating print parameters on part quality will be discussed as well as the ability of these structures to effectively and efficiently absorb energy.

In order to assess the energy absorbing potential of the 3D printed structures, it is necessary to understand their compressive behaviour. Figure 2 shows the typical compressive behaviour of three cellular structures, in this case foams [18], with different densities. In each case, three deformation regions can be observed: linear elasticity, plateau and densification. At small compressive strains, the behaviour is linear as the cell walls of the structure are undergoing simple bending. As deformation progresses, the cell walls begin to buckle which produces the characteristic plateau and then finally, the opposing cell walls come into contact and densification occurs; at densification the stiffness of the structure increases steeply, tending to the stiffness of the parent material.

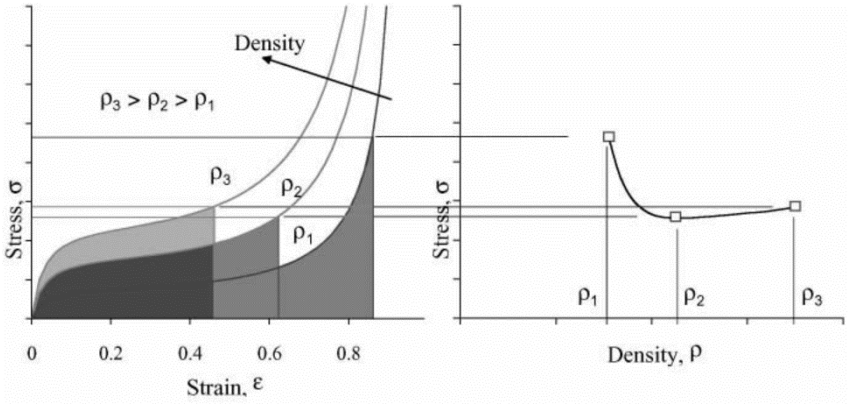

Figure 2: Stress strain curves of typical foams of different density with stress transferred for the same impact energy [16]

The energy absorbed by a cellular structure during a compression is simply the area under the stress strain curve, up to the strain, ε, to which it is compressed. Since very little energy is absorbed in the linear region, it is a long flat plateau that is desired for an efficient energy absorbing structure, such that compressive energy can be absorbed at a near constant load. In Figure 2 the shaded regions under each curve represent the same amount of energy, indicating the stress, σ and strain, ε that would be reached, should each of the structures be compressed by the same compression event. It can be see here that the structure with the intermediate density, ρ_2 transfers the lowest stress whilst the structure with the lowest density, ρ_1 has begun to densify, transferring a much higher stress. The high density structure has a higher plateau stress and as a result also transfers a higher stress; it can therefore be said that the structure with the intermediate density is optimised for absorbing this energy. There exists a compression energy to which any uniform-density cellular structure is uniquely optimised, and identifying this is one of the methods for quantifying the energy absorbing capability and efficiency of a cellular structure; applying this analytical methodology to 3D printed constructs permits unique tailorability of the response to the environmental loading. From a designers point-of-view, the stress-strain diagrams for each 3D printed structures will generate energy absorption and efficiency diagrams which can be employed as part of a designer's toolbox to characterise the energy absorbing potential of cellular structures [18,19].

Materials and methods:

3D printing of cellular structures

The cellular structures in this study were produced via FFF 3D printing using the Ultimaker Original desktop 3D printer shown in Figure 1c. Two grades of TPU filament produced by Fenner Drives Inc were used as feedstock material: low stiffness NinjaFlex filament and the comparatively stiff SemiFlex material. Both materials have the same density, ρ_S=1235 ±3 kg/m^3. Differential scanning calorimetry was carried out on samples of the filaments in order to assess the most appropriate melt temperature of the materials to ensure print quality and avoid thermal degradation of the materials

during print. As a result of the study, the temperature of the extruder was set to 227°C. As well as extruder temperature, print parameters such as extrusion rate, layer height and print head speed all affect the final print quality of these parameters were optimised in a prerequisite testing campaign, for prints that contained the lowest void fraction.

Tensile tests of the TPUs were carried out on straight specimens in accordance with ASTMD412 [20]. The specimens were produced via 3D printing with optimised print parameters, with the primary print direction at 0° to the specimen extension direction. The tensile behaviour of both TPUs is linear at low strains transitioning into lower stiffness, highly non-linear behaviour at strains, $\varepsilon>0.03$. The low strain modulus for the NinjaFlex and the SemiFlex tested were $E_N=26.5N/mm^2$ and $E_S=89.5N/mm^2$ respectively. At nominal strains of $\varepsilon=1$ and $\varepsilon=2$ the nominal stress in the NinjaFlex specimens were $\sigma_{N\_1}=5.12N/mm^2$ and $\sigma_{N\_2}=5.96N/mm^2$ respectively and the nominal stress in the SemiFlex specimens, $\sigma_{S\_1}=11.62N/mm^2$ and $\sigma_{S\_2}=13.63N/mm^2$ respectively; such that at these points, $\sigma_N=0.44\sigma_S$. The tensile strength of SemiFlex material is $\sigma_S=38.4N/mm^2$; for comparison between 3D printing techniques, this is 32x the tensile strength of flexible TangoPlus material used in Polyjet 3D printing [5].

Cellular arrays:

Hexagonal arrays with a range of relative densities were formed from regular hexagonal unit cells with cell wall thickness, *t* and cell wall length, *l*. Figure 3a shows a schematic of a single unit cell. The theoretical relative density for a cellular array formed from these regular hexagons is equal to, $\rho^*_{RD}=(2/3^{-2})(t/l)$ [21] such that ρ^*_{RD} is directly proportional to the t/l ratio of a hexagonal unit cell. The measured relative density, ρ_{RD} of the final 3D printed specimens was calculated such that $\rho_a/\rho_S=\rho_{RD}$ where ρ_a=specimen mass/the cuboidal area which it occupies. The comparison of the values of ρ_{RD} and ρ^*_{RD} is one method of assessing the quality of the produced specimen compared to an idealised array.

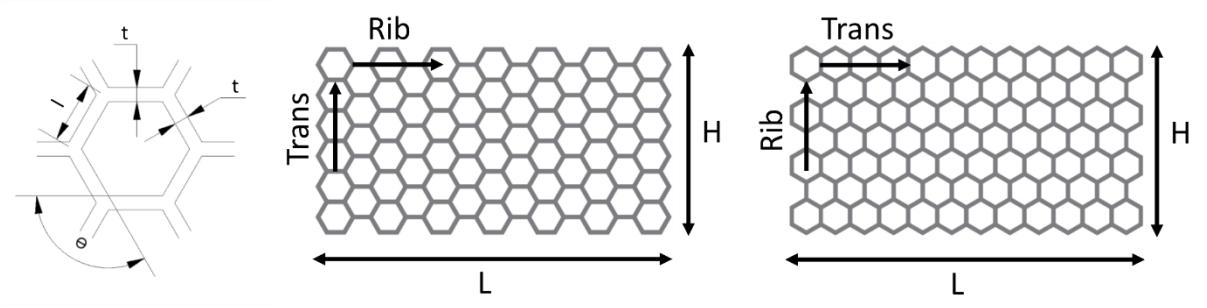

Figure 3: a) Unit cell dimensions for the repeating unit cells (Θ=60°); b) These unit cells assembled in the Ribbon and c) the transverse direction to the intended compression direction

The hexagonal unit cells were assembled into arrays, examples of which are depicted in Figure 3b and 3c. The arrays shown in 3b and 3c are assembled from unit cells 90 degrees out of phase, designed to be compressed vertically. Conventional expanded honeycomb structures are formed from ribbons of material which are expanded to form the final structure and once formed, the direction with which the ribbon material is aligned is referred to as the “ribbon” direction and orthogonal to this is the “transverse” direction. For clarity in discussion, from herein this nomenclature shall be adopted such that the sample assembled in the orientation shown in 3b is designed to be compressed in the transverse direction and the structure shown in 3c, in the ribbon direction. Samples were designed to have a larger length, *L* compared to height, *H* in order to avoid global buckling of the sample in compression and reduce the effects of the vertical free boundaries on the global compressive

behaviour. Global sample dimensions *L, H* and depth, *D* were chosen as a trade-off between realising a large number of cellular rows and achieving a reasonable time of manufacture.

Compression tests:

The aims of mechanical testing in this work were threefold. Firstly, to establish the durability of structures, assessing their ability to withstand multiple compressions to densification. Secondly, to establish the stress-strain profile of these structures under compression in the Ribbon and Transverse directions, thus allowing an assessment of their comparative energy absorbing capabilities. Finally, to study the effect of strain rate and strain history upon the energy absorbing capability of these structures.

Compression tests were carried out on an Instron 3343 Universal testing machine with a 1kN load cell and a Shimadzu AGS-X with a 10kN load cell at room temperature. The unconstrained samples were compressed between flat steel plates at constant strain rates of 0.03, 0.095 and $0.3s^{-1}$ to the point of full densification and then unloaded at the same rate; this loading and unloading cycle was repeated 5 times for each sample and with tests controlled and recorded using Bluehill and Trapezium X software for the Instron and the Shimadzu test machines respectively. All data was captured at a minimum sampling frequency of 10Hz. The deformation behaviour of all the specimens was recorded using a video gauge which also recorded the position at the plate surface using a speckle pattern on the face of the compression plates; this measurement was used to verify the positional location recorded direct from the test fixture.

Nominal strains, ε of the samples were recorded by measuring the change in deflection at the interface of the samples with the steel plates and nominal stress, σ by dividing the recorded force by the initial projected area, *D x L* of each sample. By formulating stress strain curves from data gathered in this way, it is possible to extrapolate the energy absorbing capability and energy absorbing efficiency of these structures. All data was post processed using MATLAB software.

Results and Discussion

Sample quality

Our aims were to create cellular structures which a) could be repeatedly produced within a close tolerance to their design dimensions, b) were absent of defects which could significantly affect their mechanical properties, c) could be produced in a reasonable time frame such that this manufacturing method can be scaled to larger structures and d) could be capable of withstanding repeated compressions to full densification without degradation.

Figure 4a shows a honeycomb structure printed from TPU (ρ_{RD}=0.26) with optimised print parameters and for reference, in 4b a flat plate is shown which was printed with print parameters which result in a part with reasonable surface finish but which impart voidage often seen in FFF printed parts.

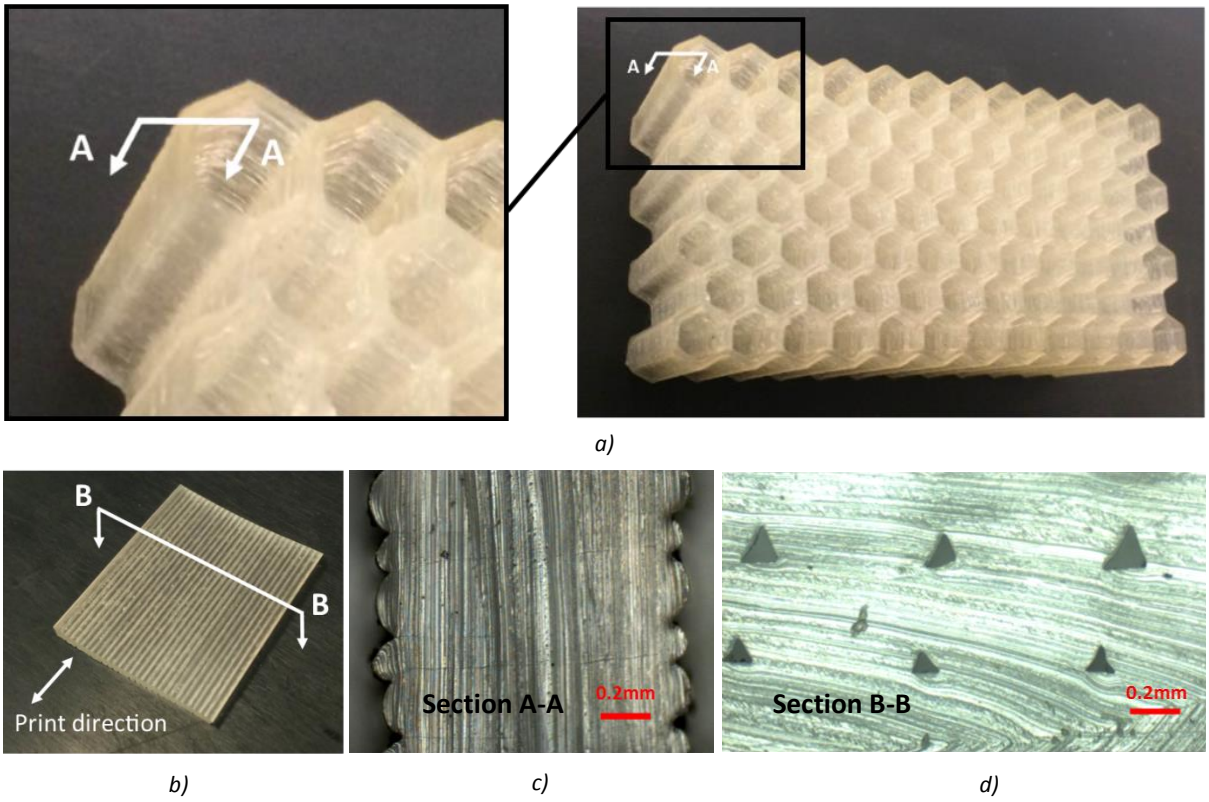

Figure 4: a) 3D printed TPU honeycomb (ρ_{RD}=0.26) with magnified image of section A-A; b) Flat plate printed from TPU with non-optimised print parameters; c) Section A-A, a cross section of a typical cell wall from a cellular structure with optimised print parameters, print direction into the page, two adjoining extruded lines and 0.8mm nozzle diameter; d) Section B-B showing voidage, with the print direction into the page, nozzle diameter 0.8mm

It can be seen in section A-A (Figure 4c) that the cross section of a cell wall of a hexagonal sample with optimised print parameters does not contain any of the type of voidage that can occur at the intersection of lines of filament such as seen in section B-B (Figure 4d); the print direction of these section views is into the page and each layer of section A-A is made up from two lines of filament which have joined at the centreline.

Voidage was eliminated in 3D printed parts by extruding more material than dictated by the internal volume of the CAD model during printing, allowing the print head to smear the bond line. This was achieved by lowering the layer thickness to 0.2mm whilst maintaining a higher extrusion rate. This practice, although improving sample quality, resulted in cell walls on average 84% thicker than designed and therefore the measured density of the final arrays greatly exceed the density of the CAD generated arrays; the final manufactured samples were denser than the CAD models by a scale factor of 1.64±0.087. It must be noted that Cura slicing software was used to convert all CAD models into 3D printer toolpaths and it was in the user interface within this software that the flow rate and layer heights were manipulated to achieve the best quality samples. Different slicing software packages will inevitably produce different toolpaths for the same CAD model and therefore produce specimens of different quality. In order to consistently produce structural honeycombs via FFF from soft filament, which are true to dimensions of the CAD model, the authors are undertaking the development of a bespoke, structural honeycomb slicing software.

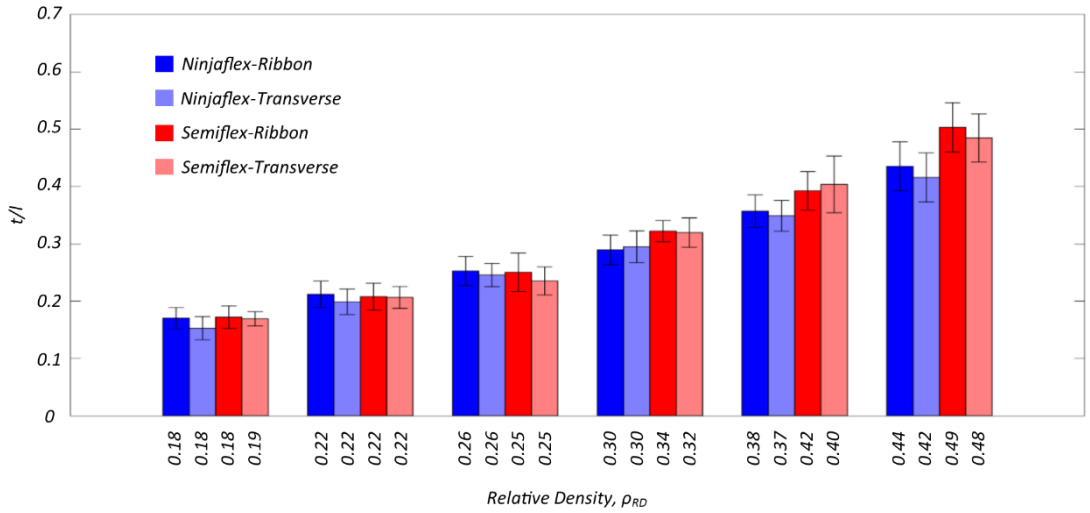

Figure 5: Average t/l ratio for members measured in each sample with maximum and minimum values recorded. Measured relative densities, ρ_{RD} of the samples are included on the x axis

Due to the flexibility and compressibility of the TPU filament, it was found that when using a Bowden-style extrusion mechanism such as that fitted to the Ultimaker 3D printer, the actual extrusion flow rate of molten TPU material can vary during a print and this effect is amplified at higher print speeds. It is believed that variations in material flow rate had a noticeable effect on the cell wall thickness, *t*; over-extrusion of the filament would lead to overly thick cell walls. Variations in flow rate do not affect the cell wall length, *l* which is instead dependent on the positional tolerances of the extruder carriage. A calibration protocol was adhered to before each print to ensure positional accuracy of all the printer components and as such, the positional error of the print carriage may be considered negligible when compared to the variations in *t.*

In order to produce specimens with a range of different densities, CAD models were assembled from six hexagonal different unit cells resulting in arrays with *t/l* ratios over the range of 0.18-0.5. Four samples were therefore produced with each design density; one to be compressed in the ribbon and one to be compressed in the transverse direction for both NinjaFlex and SemiFlex TPUs.

Figure 5 shows the average *t/l* ratios as measured in 10 members in the produced samples along with error bars indicating one standard deviation; the ρ_{RD} of each sample is indicated along the x axis. The bars in Figure 5 are grouped into samples that were produced using the same CAD model and therefore actual variations in density arise from variations in material flow rate in manufacture. It is clear that lower density structures have a lower variation in wall thickness due to a fine nozzle being used to print the lower wall thicknesses. For higher density structures, larger *t* values required a larger nozzle to be used to print the specimens within the desired time frame, trading off with cell wall thickness variation; the use of a larger diameter nozzle also results in a rounding of the cell wall corners. The measured relative density of these structures designed with the same topology varies by as much as 0.06 in the highest density group. It was found that SemiFlex samples printed with the same print settings and design topology would be produced with a higher density, which is likely caused by better gripping of the stiffer filament in the extruder mechanism, leading to a comparative over-extrusion. By utilising a direct drive style extruder, which reduces the length of filament being compressed, the flow rate of the material can be more accurately controlled. As a result of this work, a number of modifications have been made to the 3D printer and the 3D printing process which will allow the ongoing improvement of sample quality. The measured relative densities of the structures do not scale, in all cases, with the measured *t/l* ratio and this occurs due to over-extrusion which

does not contribute to thickening of the walls but rather, beads of material forming on the structures, increasing the measured relative density.

In order to meet our aim for reasonable time to manufacture, any single print was restricted to a maximum of 4 hours. This target was achieved with half of the samples being manufactured in under 2 hours, whilst maintaining reasonable dimensional tolerances.

No defects were observed under visual inspection of the structures and no failure of the specimens was observed during compression testing. Changes in the mechanical properties of the cellular structures upon repeated compressions will be discussed later.

Cellular collapse behaviour

The mechanics of hexagonal structures are well understood and their deformation behaviours under different loading conditions have been established via mechanical models [19,20]. At low strains, the cell walls of a regular hexagonal array loaded in either the transverse and ribbon direction will deform by bending as illustrated in Figure 6a and 6b respectively [21]. As compressive strains become large, hexagonal honeycombs compressed in the ribbon direction will begin to buckle in a manner illustrated in Figure 6c; for honeycombs with a $t/l<1/4$ this occurs at approximately ε=0.1 [21]. For samples compressed in the transverse direction, the walls continue to bend and buckling does not take place. Mechanical models of honeycombs have been validated experimentally by Gibson *et al* who carried out compression tests on metal and moulded silicone rubber honeycombs [22]; the eight mechanical properties assessed experimentally were in good agreement with the developed theory.

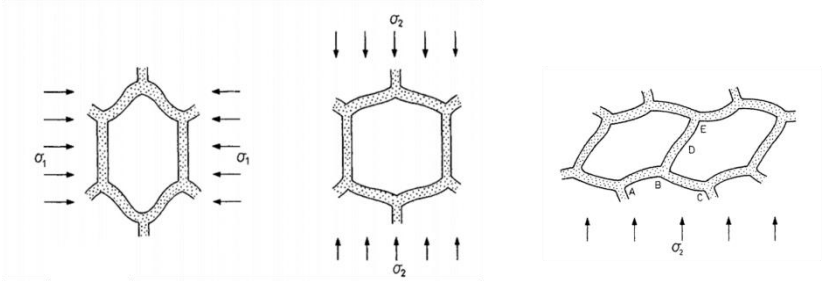

Figure 6: Compression behaviour in bending of unit hexagonal cells compressed in the a) Transverse and b) Ribbon direction; c) the buckling behaviour of unit cells compressed in the Ribbon direction. Adapted from [16]

The value of assessing the deformation patterns of our 3D printed specimens is to identify possible areas of poor print quality which would likely result in a deviation from the expected deformation behaviour and to assess the effect of the edge loading conditions on global deformation behaviour. It must also be noted that some of the honeycombs produced have a high density where $t/l>1/4$ ($\rho^*_{RD}>0.29$) and in these cases, the assumptions made in mechanical models of honeycombs are no longer valid, as the cell walls can no longer be assumed to undergo simple buckling behaviour [18]. It cannot be assumed that the high density honeycombs will behave in the same manner as predicted for those with slender walls.

Figure 7a and 7b show the deformation behaviour of SemiFlex TPU samples, on the 5th compressive cycle, in the ribbon (ρ_{RD}=*0.49*) and transverse (ρ_{RD}=*0.48*) directions respectively, at strains of 0, 0.15, 0.32 and 0.55. Despite their high density, the deformation patterns are consistent with those predicted for honeycombs with slender cell walls; the vertical columns behave like end loaded struts, connected at a node, with a certain rotational stiffness [21]. At a strain of 0.15, the cell walls which were initially aligned vertically in the sample compressed in the ribbon direction have rotated and have reached the point of elastic collapse, now undergoing the buckling behaviour depicted in Figure 7c. The vertical members in the central most rows of this sample are the first to deform and rotate which is due to the constraint induced on the outermost rows by the plate contact; because of the flattening of the outer cell wall at the plate, the nodes along this edge have a higher rotational constraint than the central nodes. This edge restriction in deformation is not seen for the sample compressed in the transverse direction, where deformation is more pronounced at intermediate strains at the rows in contact with the plate. In order to reveal more about the deformation mechanisms across the range of samples, it is necessary to examine their compressive stress-strain response.

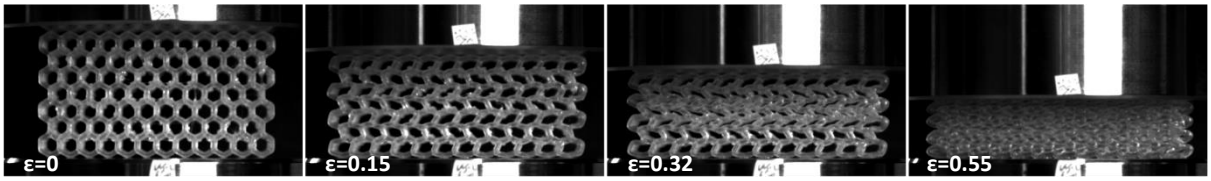

a)

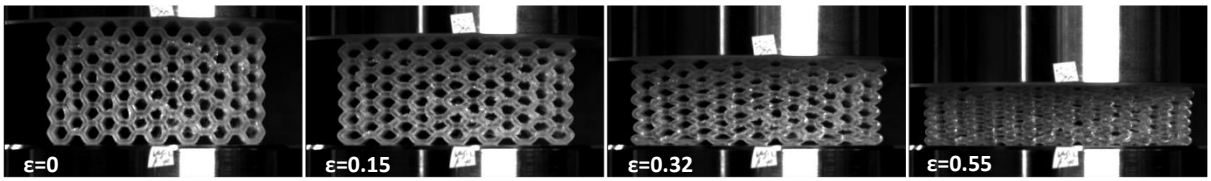

b)

Figure 7: Compressive behaviour of SemiFlex TPU samples, on the 5th compressive cycle, in a) the ribbon (ρ_{RD}=0.49) and b) transverse (ρ_{RD}=0.48) directions. Strains from left to right of 0, 0.15, 0.32 and 0.55.

Stress Strain behaviour

In Figures 8a-d, the static compression stress-strain curves are plotted for all arrays at a strain rate $\dot{\varepsilon}$=0.03s^{-1}. Figures 8a and 8b contain data for NinjaFlex and SemiFlex arrays compressed in the ribbon direction respectively, and 8c and 8d are for the NinjaFlex and SemiFlex arrays compressed in the transverse direction respectively. Each plot contains data for six arrays with different densities and in all cases an increase in density corresponds to decrease in strain to densification, an increased plateau stress and decrease in plateau length. All stress-strain curves are smooth in character and do not exhibit undulations which are characteristic of the staggered collapse behaviour of honeycombs undergoing plastic deformation [23]. Although the curves for all arrays show three distinct regions of linear deformation, low stiffness plateau and high stiffness densification, due to the different deformation mechanisms at a unit cell level, there are some key differences in the curve shapes for the samples compressed in the ribbon and transverse directions. Compression in the ribbon direction results in a flatter plateau and the transverse compression results in a more marked increase in stress over the plateau region, even for low density samples. The transition to the plateau region from the linear elastic region is more abrupt in the samples compressed in the ribbon direction caused by the presence of buckling behaviour.

The point of maximum energy absorbing efficiency for each sample is found at the stress where the increase of energy absorbed by the structure (increase in the area under the stress strain curve) is exceeded by the corresponding stress increase [18]; the energy absorbing efficiency of these structures shall be discussed in greater detail in the next section where define a numerical "efficiency parameter" shall be defined. These points have been included in Figure 8 as they provide a strain value at which the onset of densification can be defined. For samples compressed in the transverse direction, these points occur at higher strains, indicating a higher strain to densification for samples with the same density.

The stiffness of the TPU used to form the array does not affect the characteristic shape of the stress strain curve but instead scales the stiffness response, as can be seen by comparing nested curves in 8a and 8b or 8c and 8d; note the change in y-axis values.

In order to effectively assess the energy absorbing behaviour of these structures, it is necessary to display this data more intuitively, in the form of efficiency diagrams.

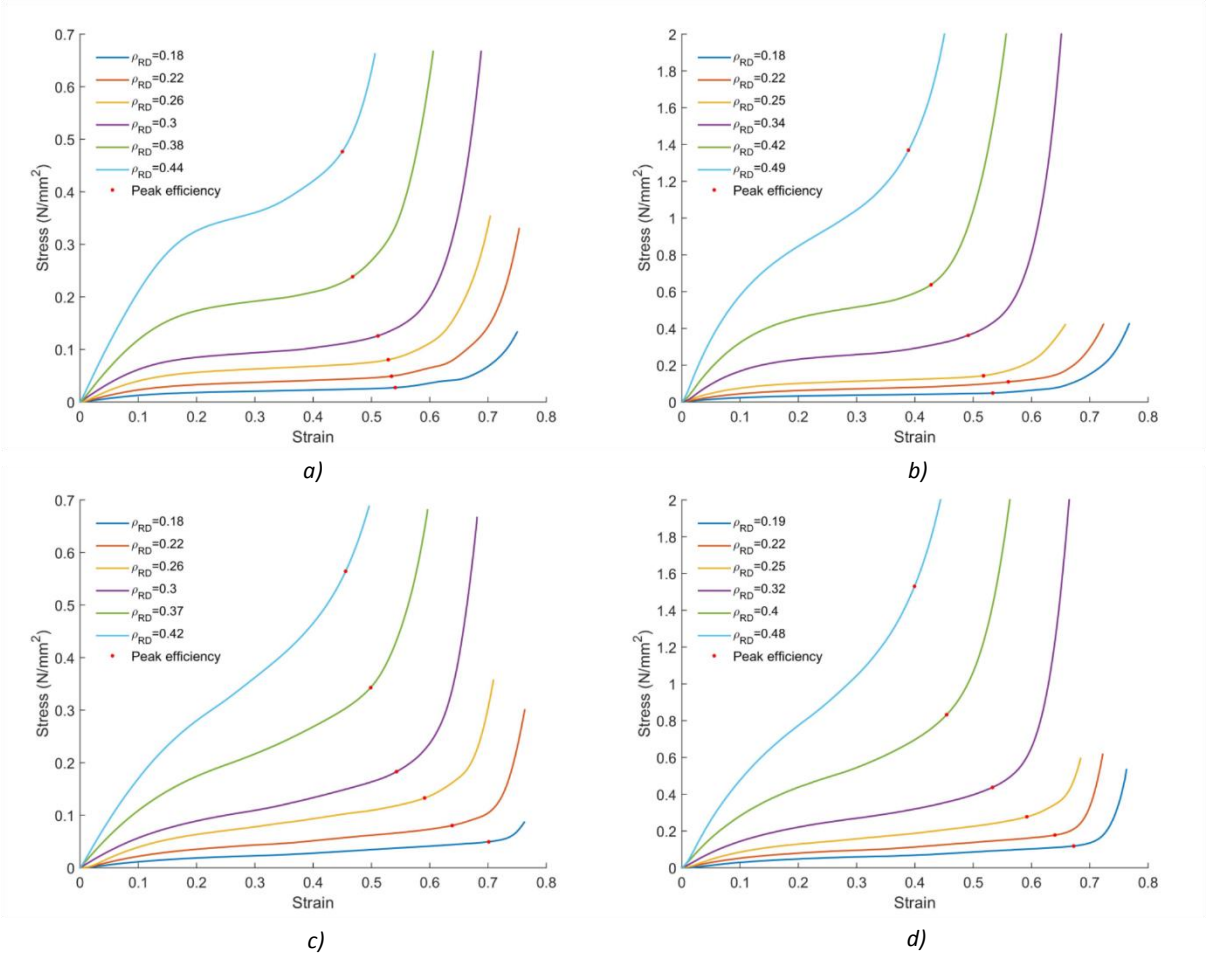

Figure 8: Stress strain behaviour of hexagonal arrays formed from a) NinjaFlex and b) SemiFlex compressed in the Ribbon direction and samples formed from c) NinjaFlex and d) SemiFlex compressed in the transverse direction

Energy absorption efficiency

The efficiency of a structure at absorbing energy can be described by an 'efficiency parameter', which is the ratio of cumulative absorbed energy up to a given stress, divided by the stress [21], see Equation 1:

$$E = \int_0^{\varepsilon} \frac{\sigma(\varepsilon)d\varepsilon}{\sigma} \qquad \text{Equation 1.}$$

This efficiency for a given structure under compression will have a maximum at a single point as previously discussed and will take a value between 0-1. In reality, it is not possible to have a structure with a maximum efficiency of 1 since this would require the structure to collapse with infinite stiffness to a horizontal plateau and densify at a compressive strain of 1; the efficiency parameter effectively compares the energy absorbed by a practical structure to this "ideal" energy.

Figure 9a-d shows the efficiency-stress curves for the TPU structures compressed at strain rate, $\dot{\varepsilon}$=0.03; these correspond directly to the results shown in Figure 8a-d. In each case, the iso-energetic contours which correspond to the maximum efficiency of each sample density are also reported. The maximum energy absorbing efficiencies of all hexagonal structures assessed in this study are between 0.2-0.4 and decrease non-linearly with increasing density. Although these values may appear low, it should be noted that a structure that densifies at a strain of 0.5 would be limited to a maximum efficiency value of 0.5, should it undergo ideal behaviour to this point; in work by Avelle *et al.* [18], the energy absorption efficiency of structural foams ranged from 0.3-0.5.

For the case for NinjaFlex arrays compressed in the ribbon direction (Figure 9a), the three lowest density arrays (ρ_{RD}=0.18, 0.22 & 0 .26) have a constant maximum efficiency of 0.36. This efficiency drops to 0.33, 0.31 and 0.28 for three higher density samples with ρ_{RD}=0.3, 0.38 & 0 .44 respectively. By referring to the stress-strain diagram in Figure 8a, the efficiency reduction can be explained as the plateaus of the higher density arrays having a higher positive gradient, becoming increasingly distorted from the ideal compressive profile. This drop in efficiency occurs for arrays with $\rho_{RD}>0.29$ corresponding to where, as previously discussed, the cell wall members can no longer be considered as undergoing simple buckling behaviour.

For equivalent structures formed from SemiFlex shown in Figure 9b, arrays with relative densities, ρ_{RD}=0.18 and 0.25 also show a maximum efficiency of 0.36 and there is a clear decrease in efficiency of the higher density samples thereafter. The sample with ρ_{RD}=0.22 has a lower than expected efficiency value of 0.34. Upon observing video footage of the samples compression, it is clear that the edge loading conditions had a large effect on the staggering the collapse behaviour of this sample which is reflected in the uneven stress-strain plateau profile. As the sample with the smallest height, H, it is the most susceptible to these effects and repeat tests should be carried out on similar specimens with a larger number of rows to confirm that this is indeed the case. To address this point, an experimental campaign investigating the effects of boundary conditions on samples of varying thicknesses is currently being undertaken by the authors and will be reported separately.

As shown in Figures 9c and 9d, the efficiency of the lowest density NinjaFlex and SemiFlex specimens compressed in the transverse direction have peak efficiencies of 0.37 and 0.36 respectively and for both materials the peak efficiency values decrease non-linearly with increase in density. The decrease in peak efficiency with increased density is greater for these specimens compressed in the transverse than for the samples compressed in the ribbon direction.

The arrays compressed in the ribbon direction absorbed less energy per volume at their peak efficiency than the arrays compressed in the transverse direction when compared like for like with

density. In the case of the sample compressed in the ribbon direction with ρ_{RD}=0.22, the equivalent sample compressed in the transverse direction absorbed 56% percent more energy at peak efficiency. The SemiFlex sample with ρ_{RD}=0.22 compressed in the transverse absorbed 77% more energy at peak efficiency than the equivalent sample compressed in the ribbon direction. It must be noted that, although more energy is absorbed per unit volume up to densification for the samples compressed in the transverse direction, the stresses transferred by the structure are also higher, leading to a similar or lower value in efficiency than the equivalent structures compressed in the ribbon direction. In order to better assess the energy absorption capacities of these structures, it is advantageous to plot energy absorption diagrams. This diagrams also allow the direct analyse of the effect of strain rate on energy absorption behaviour.

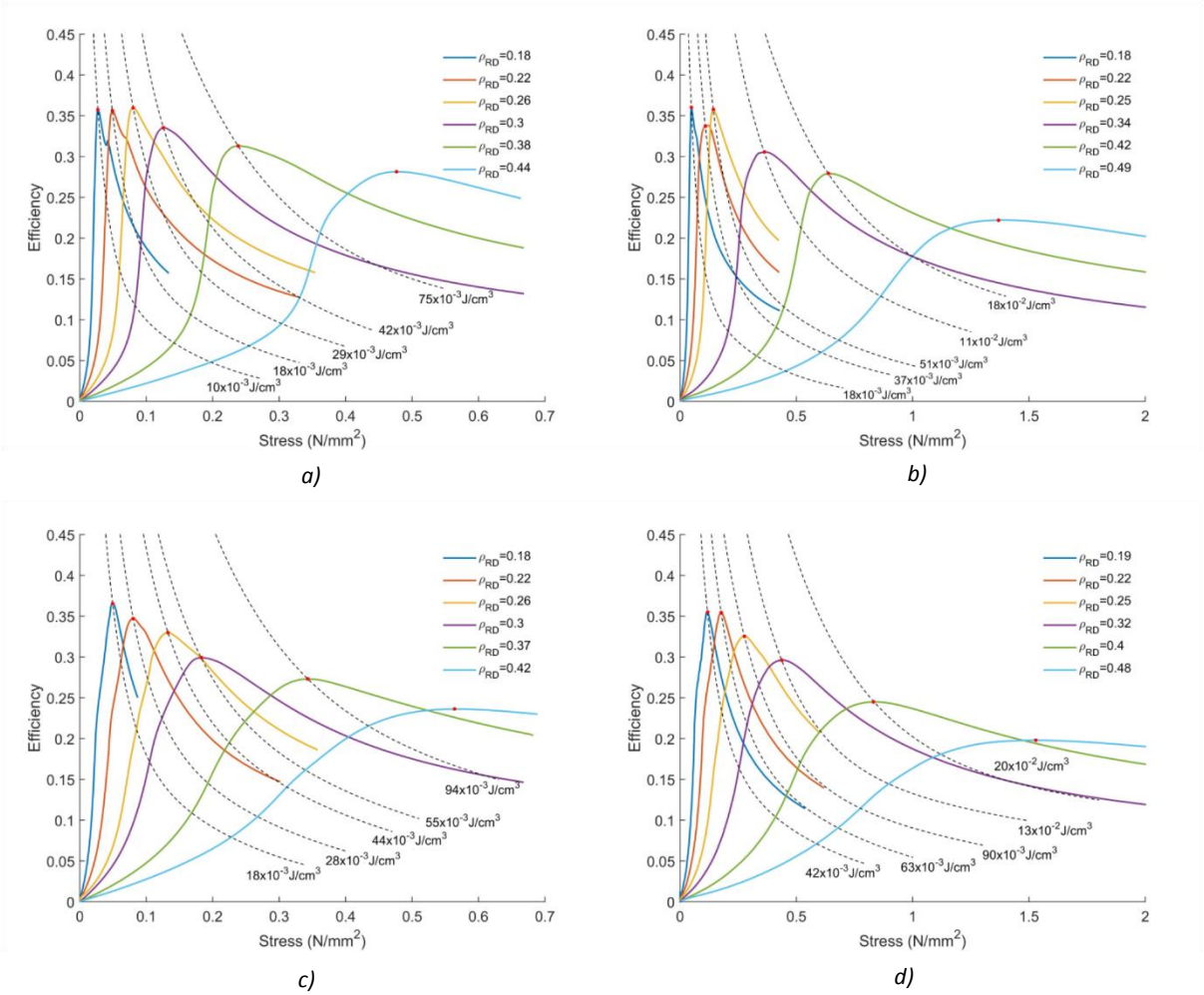

Figure 9: Efficiency-stress diagrams of hexagonal arrays formed from a) NinjaFlex and b) SemiFlex compressed in the Ribbon direction and samples formed from c) NinjaFlex and d) SemiFlex compressed in the transverse direction

Energy absorption diagrams

An effective energy absorbing structure will completely absorb the kinetic energy of a moving body whilst keeping the force on the body below a certain level. In order to assess the energy absorbing event the different cellular structures would be optimised for, Figure 10 shows the specific energy absorbed by the different arrays at their maximum efficiency as a function of applied stress. These energy absorption diagrams allow us to plot the results for multiple strain rates and therefore assess how material viscoelasticity effects the energy absorbing behaviour. It must be noted that for polymeric foams, more energy is absorbed at higher strain rates in part due to the damping effect of fluid flow within the porous material [21] however, due to the large length scale of the cells in these structures, any strain rate dependence is entirely due to the viscoelastic nature of the material.

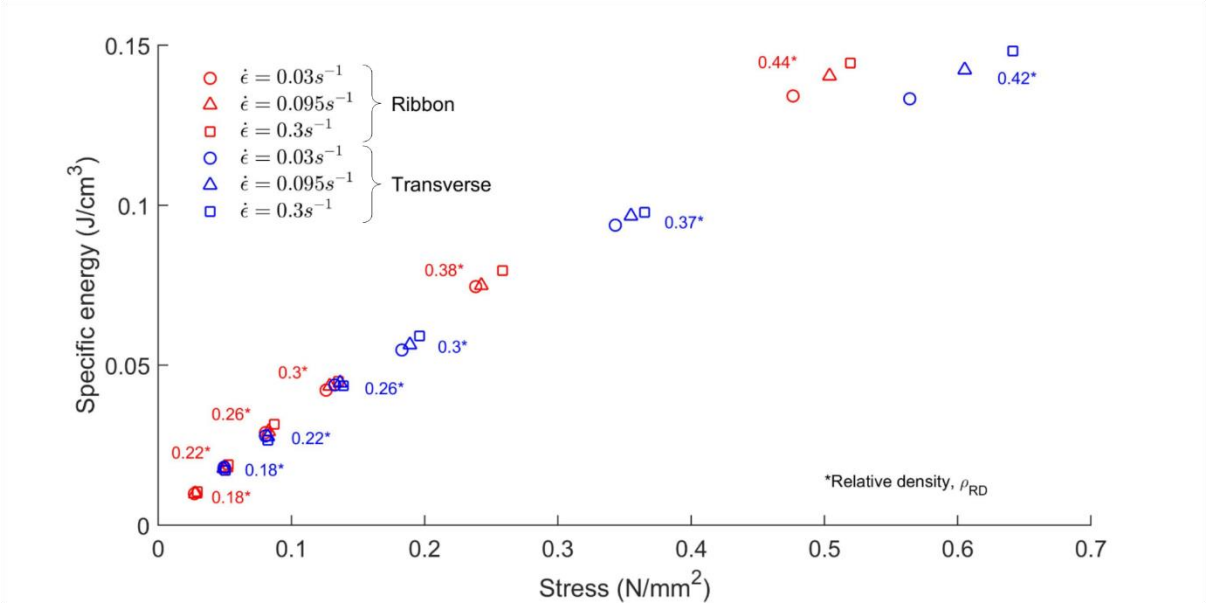

a)

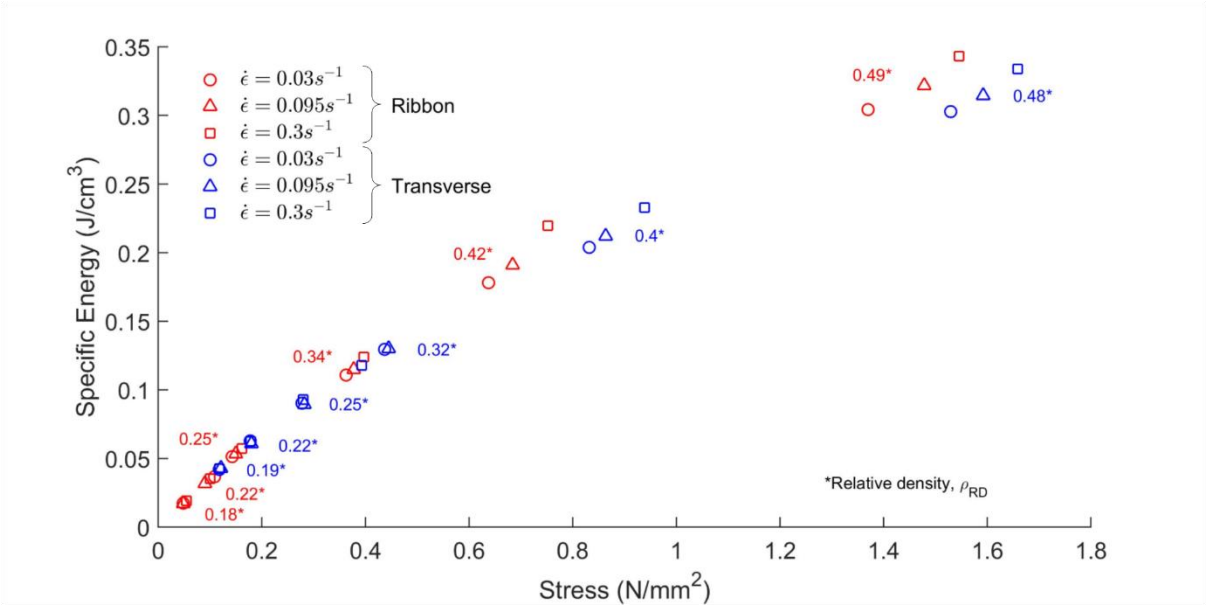

b)

Figure 10: Energy absorption diagrams for a) NinjaFlex hexagonal arrays and b) SemiFlex hexagonal arrays compressed at strain rates of 0.03, 0.095 and 0.3s^{-1}

For both grades of TPU, with samples increasing in density, increase in energy with stress transferred is non-linear such that, if an envelope were to be drawn though the points of a single structure at a single strain rate, a decreasing gradient would be observed. This decreasing gradient reflects the decrease in efficiency of these structures with increasing density, noting that the peak efficiency of any structure may be found, using this diagram, by dividing the energy by the stress at any of these points.

Figure 10 indicates there is a clear strain rate dependency in these structures, with increased strain rate leading to increased energy absorption and increased stress transferred; this rate dependency increases for samples with higher density. Here, the rate dependence has been studied over one order of magnitude and at relatively low rates. It is important that higher strain rates over a wider range are studied in future to allow conclusions to be drawn with regards to how these structures will behave under impact conditions.

These diagrams provide benchmark energy absorption envelopes for honeycomb structures formed from TPU via 3D printing. The area of the graph to the left of the envelope formed by the energy-stress points is inaccessible for honeycomb structures formed from these topologies, from these materials at the strain rates studied. For example, it would not be possible to use a hexagonal honeycomb structure made from either of these TPUs to absorb 0.1J/cm^3 whilst transferring a stress of 0.2N/mm^2. Finally, it should be noted that the data shown here is for the 5th compressive cycle of these structures and for materials such as these TPUs, strain history may have a significant influence on their energy absorbing capability.

Cyclic softening behaviour

In static compressive testing of TPU, it has been observed that the material will undergo a softening behaviour as the loading and unloading process is repeated [14]. When compressed at strain rates of 0.01s^{-1}, Qi and Boyce [14] observed that the stress-strain curve in the second cycle was far more compliant than in the first for solid TPU specimens. Furthermore, reduced strain softening behaviour was observed in subsequent cycles, with the behaviour stabilising after four cycles; the authors noted that the unloading curves were seen to follow the same path regardless of loading cycle.

This phenomena is due to the potential for strain softening behaviour in TPUs; in our study the specimens were loaded for 5 consecutive cycles in all tests, since this allowed direct observation on how the material behaviour may affect and influence the energy absorbing potential of the hexagonal arrays. Figure 11a reports the stress-strain behaviour of the SemiFlex array with ρ_{RD}=0.34 loaded and unloaded over 5 cycles in the ribbon direction at a strain rate of 0.03s^{-1}. As seen for neat TPU, the array is much more compliant on the second cycle than the first with the behaviour beginning to converge after 5 cycles. In these samples, a slight reduction in compliance was also seen in the unloading cycle; a behaviour not see when neat TPUs were unloaded in compression tests by Qi and Boyce [14].

It was also observed that after each successive compression, the height of the specimen did not return to the original full height. This behaviour was almost entirely a viscoelastic effect rather than plastic deformation as all samples returned to within 1% of their original height, H after one hour. In all previous data presented for the 5th compressive cycle, this residual deflection was factored into the value of compressive nominal strain. The first compressive cycle does not have the same smooth profile as the subsequent cycles with a number of undulations along the stress plateau. This behaviour occurs during the first loading cycle where cellular collapse is much more staggered and less uniform across the rows of the array.

Figure 11b shows the energy absorbed by the array up to a compressive strain, ε_{max}=0.7 on each successive compressive cycle. The reduction in the amount of energy absorbed after the first compression is 24.5% and this reduces to a 1.6% reduction after the forth compression. It is clear that the performance of these structures in terms of total energy absorbed per cycle is significantly degraded after the first cycle but quickly converges. It can also be observed that the damping capability of the structure, which is proportional to the area encapsulated by a full loading and unloading cycle, is significantly reduced after the first cycle. These strain softening effects are also present in samples manufactured from NinjaFlex TPU but to a lesser degree; the equivalent sample manufactured from NinjaFlex absorbed 15.3% less energy on the second compressive cycle when compressed under the same conditions.

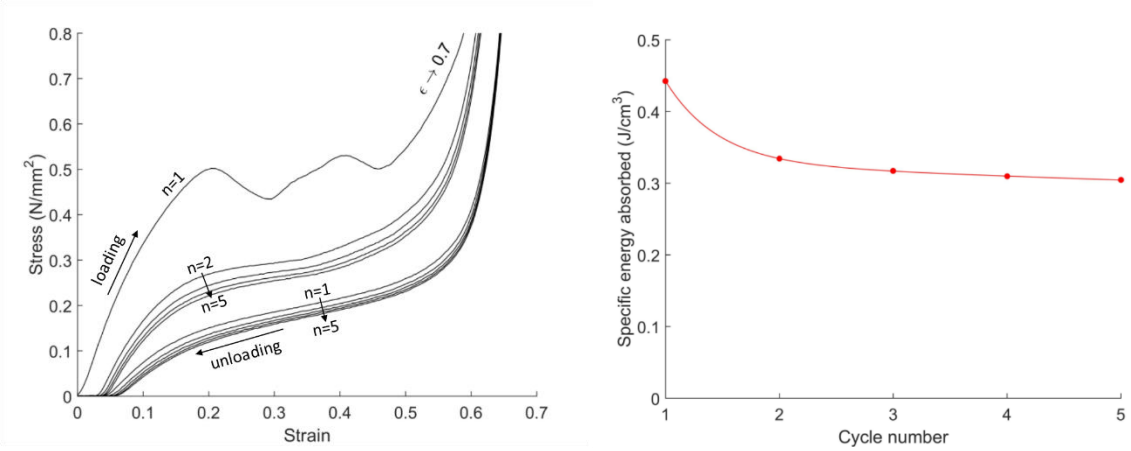

a) *b)*

Figure 11: a) Stress strain curves for the loading and unloading cycles n=1-5 for SemiFlex sample, ρ_{RD}=0.34 at a strain rate of 0.01s^{-1} and b) the energy absorbed on each compressive cycle with percentage reduction indicated

Conclusions

In this work we have shown that it is possible to produce resilient, hyperelastic, energy absorbing structures via the method of FFF 3D printing. By utilising commercially available thermoplastic polyurethane as a parent material it was possible to form structures which could be repeatedly compressed without fracture, and by optimising our printing technique all visible voidage was removed in the samples analysed.

The room temperature mechanical properties of hexagonal arrays formed from two types of commercially available TPU (namely NinjaFlex and SemiFlex) were examined, repeatedly compressing the structures in the ribbon and transverse directions over strain rates 0.03-0.3s^{-1} to densification. By forming stress-strain diagrams, efficiency diagrams and energy absorption diagrams, were able to analyse the energy absorbing potential of hexagonal arrays with relative densities ranging from 0.18-0.49 and establish the critical difference in mechanical behaviour of these arrays under different orthogonal loading conditions.

Through examination of video data, it was observed that loading the hexagonal structures in the ribbon direction resulted in a deformation pattern whereby members aligned with the loading direction would undergo elastic collapse and the nodes at which they were attached would then rotate. This collapse behaviour is consistent with that presented in [21] and was seen even in samples with high density (ρ_{RD}>0.29). The resultant stress-strain profile has a characteristic long, flat plateau desired for energy absorbing structures and as such, peak energy absorbing efficiencies of 0.36 were realised. The absence of a similar buckling mechanism in the samples loaded in the transverse direction resulted in a plateau with a higher positive gradient and densification at a

higher nominal stress but also higher nominal strain; peak energy absorbing efficiencies of 0.36 were also realised for low density samples compressed in this manner.

Upon repeated compression of all TPU honeycombs, dramatic cyclic softening behaviour occurred, with up to a 25% reduction in energy absorption observed from the first to the second compressive cycle (ε_{max}=0.7). This behaviour has been observed in neat TPU but must be further studied in these structures as the effect is likely to be dependent on a number of aspects of the strain history.

This research demonstrates the potential for 3D printed, hyperelastic honeycombs as energy absorbing structures, with the structures created meeting the criteria of resiliency, good energy absorbing efficiency and quality of manufacture. The structures in this study take the form of one of the most basic of potential energy absorbing structures. In the future, we can now begin to realise the potential of this 3D printing manufacturing method for forming structures which are highly tailored to specific energy absorbing tasks by including cellular hierarchy, density grading and novel architectures. Further investigations into the complex behaviour of the TPU parent material, which include cyclic softening, shall be conducted as well as high strain rate and impact analysis of the honeycomb structures. The FFF 3D printing process used in this study is inexpensive, fast and has permitted the authors to generate the first 3D printed cellular structures capable of withstanding repeated compression cycling to densification. With further optimisation, this printing technique and the use of TPUs holds excellent potential for creating high performance, tailored energy absorbing structures for extreme environments.

Acknowledgements

This work is financially supported by the Engineering and Physical Sciences Research Council through the EPSRC Centre for Doctoral Training in Advanced Composites for Innovation and Science (grant number EP/G036772/1) and the Royal National Lifeboat Institution (RNLI). The Authors would like to thank the RNLI for their continued support and involvement with the progression of this work.

References

[1] H. W. Bixby, Development of a Paperboard Honeycomb Decelerator for Use with Large Platforms in Aerial Delivery Systems, WADC'TR 59-776, Wright Air Development Center, Wright-Patterson AFB, Ohio, (1959)

[2] R. K. McFarland, Jr., The development of Metal Honeycomb Energy-Absorbing elements, Technical report No. 32-639, Jet propulsion Laboratory, California Institute of Technology, (1964)

[3] S.D. Papka, S. Kyriakides, In-plane biaxial crushing of honeycombs – Part I: Experiments, International Journal of Solids and Structures (1999) 4367–4396

[4] S. D. Papka, S. Kyriakides, In-plane crushing of Honeycombs – Part II: Analysis, International Journal of Solids and Structures, *36*, pp. 4397-4423 (1999)

[5] K. Wang, Y.-H. Chang, Y. Chen, C. Zhang & B. Wang, Designable dual-material auxetic metamaterials using three-dimensional printing. *Materials & Design*, *67*, pp. 159–164 (2015)

[6] A. Ajdari, B. H. Jahromi, J. Papadopoulos, H. Nayeb-hashemi, & A. Vaziri, Hierarchical honeycombs with tailorable properties, International Journal of Solids and Structures, *49*, pp. 1413–1419 (2012)

[7] R. Oftadeh, B. Haghpanah, D. Vella, A. Boudaoud, & A. Vaziri, Optimal Fractal-Like Hierarchical Honeycombs. Physical Review Letters, *113* (2014)

[8] J. Brennan-Craddock, D. Brackett, R. Wildman, & R. Hague, The design of impact absorbing structures for additive manufacture, Journal of Physics: Conference Series, *382,* (2012)

[9] I. Maskery, A. Hussey, A. Panesar, A. Aremu, C. Tuck, I. Ashcroft & R. Hague, An investigation into reinforced and functionally graded lattice structures, Journal of cellular plastics, 0, pp. 1-15 (2016)

[10] J. Shen, S. Zhou, X. Huang & Y. M. Xie, Simple cubic three-dimensional auxetic metamaterials. *Physica Status Solidi (B) Basic Research*, *251*(8), pp. 1515–1522, (2014)

[11] SLS system schematic by Wikimedia user Materialgeeza, CC BY-SA 3.0, Available at: https://commons.wikimedia.org/w/index.php?curid=4032088 [Accessed: 27th June 2016]

[12] 3D Systems, sPro™ 60 HD. [Image] Available at: http://www.3dsystems.com/3d-printers/production/spro-60-hd [Accessed: 4th July 2016]

[13] E3D-online, Cutaway of 3mm Bowden. [Image] Available at: http://e3d-online.com/E3D-v6 [Accessed: 4th July 2016]

[14] H. J. Qi & M. C. Boyce, Stress-Strain Behavior of Thermoplastic Polyurethane Stress-Strain Behavior of Thermoplastic, Mechanics of materials, pp. 1–51 (2005)

[15] Ö. İLKGÜN, Effects of production parameters on porosity and hole properties in laser sintering rapid prototyping process. Diss. Middle East Technical University, (2005).

[16] G. D. Kim & Y. T. Oh, A benchmark study on the rapid prototyping processes and machines: quantitative comparisons of mechanical properties, accuracy, roughness, speed, and material cost, Journal of Engineering Manufacture *222,* Part B, pp.201-215, (2008)

[17] Ultimaker Original general specifications. Available at: https://ultimaker.com/en/products/ultimaker-original#specifications [Accessed: 5th October 2016]

[18] M. Avalle, G. Belingardi, & R. Montanini, Characterization of polymeric structural foams under compressive impact loading by means of energy-absorption diagram. *International Journal of Impact Engineering*, *25*(5), pp. 455–472 (2001)

[19] J. Miltz, O. Ramon, Energy absorption characteristics of polymeric foams used as cushioning materials. Polymer engineering science, 30 (2) pp. 129-133, (1990)

[20] ASTM International, D412-06 Standard Test Methods for Vulcanized Rubber and Thermoplastic Elastomers–Tension, (2006) 1–14.

[21] L. J. Gibson, & M.F. Ashby, Cellular Solids: Structure and Properties. *Cambridge University Press*, (1999).

[22] L.J. Gibson, Mechanics of two dimensional cellular materials. Proceedings of the Royal Society of London A, 313, 509–529 (1969)

[23] S. D. Papka & S. Kyriakides, In-plane compressive response and crushing of honeycomb, Journal of Mechanical physics and Solids, *42*(10), pp.1499–1532, (1994)